Population Synthesis of Millisecond Pulsar-White Dwarf Binaries

Alexandra Wells[1], Debatri Chattopadhyay[2], and Fabio Antonini[2]

[1] *Physics and Astronomy Department; Ohio University, Athens, OH, 45701, USA*
[2] *Gravity Exploration Institute, School of Physics and Astronomy, Cardiff University, Cardiff, CF24 3AA, United Kingdom*

August 2024

Abstract

In this work, we study the formation and evolution of millisecond pulsar-white dwarf binary systems. We use archival data from the rapid binary population synthesis code Compact Object Mergers: Population Astrophysics and Statistics (COMPAS), to look at a population of neutron star (NS) + white dwarf (WD) binary systems, including during the period of NS radio emission, i.e. the lifetime of the pulsar. We identify several formation channels of these systems, described as channels of (a) no identified mass transfer, (b) Roche lobe overflow with no common envelope, (c) common envelope phase later followed by Roche lobe overflow, and (d) simultaneous common envelope and Roche lobe overflow phases. We also find that the archival data shows that the pulsars of the systems where the neutron star forms first have a longer radio lifetime than those in systems where the white dwarf forms first. We lastly find that most of the mass transfer in the model is from the stable Roche lobe overflow process, and possibly overestimates the amount of mass transfer through this mode.

1 Introduction

The behaviour of compact binaries impacts many areas of astrophysics. Through the supernovae of massive stars comes the formation of neutron stars (NS) as compact remnants. The majority of observed neutron stars are also pulsars, which are rapidly spinning, highly magnetized, and strongly emit in radio (Hewish et al., 1968).

Pulsars have a spin period and spin-down rate which can be measured with great precision. Pulsars with a spin period $P < 30$ milliseconds, known as millisecond pulsars (MSPs), have a spin period that is measurable with the precision comparable to that of atomic clocks (Hobbs et al., 2012, 2020). A culmination of these MSPs across the Galaxy can be used to detect low-frequency gravitational waves in what is called a pulsar timing array (PTA) (Hobbs, 2013; Desvignes et al., 2016; Arzoumanian et al., 2018). Additionally, MSPs in binary systems showcase the end of stellar evolution, and their properties (both orbital and stellar) tell us about their formation and evolution which can be applied to our knowledge of stellar evolution as a whole.

In a MSP binary, the neutron star (that evolves to become the MSP) forms first, descending from the initially more massive of the two stars. As the companion star evolves, it may begin transferring part of its mass to the neutron star, through processes such as Roche lobe overflow (RLOF), common envelope (CE) evolution, or others (ex: wind accretion). This causes an exchange in the angular momenta between the neutron star and the transferred mass (Alpar et al., 1982; Radhakrishnan and Srinivasan, 1982;

Bhattacharya and van den Heuvel, 1991). This then may cause the neutron star to be spun-up and can lead to a change of its magnetic field (Zhang and Kojima, 2006). This 'recycling' process spins the neutron star up to the point that the magnetic field is strong enough to produce electron–positron pairs required for radio emission, and results in a longer radio lifetime due to this shorter spin period.

This process typically occurs in low-mass X-ray binaries (LMXBs) where the donor star, often evolving into a white dwarf (WD), transfers mass to the neutron star. To date, there are over 3000 discovered pulsars, over 400 of which are millisecond pulsars. Approximately 70 percent of the discovered MSPs are in binary systems with a white dwarf. The formation of MSP + WD binaries has previously been investigated in Tauris et al. (2011, 2012).

High-frequency gravitational waves emitted by the mergers of neutron star + black hole (NSBH) binaries and by double neutron star (DNS) binaries can be detected by ground-based observatories such as the Advanced Laser Interferometer Gravitational-wave Observatory (aLIGO) (Aasi et al., 2015) and Advanced Virgo (Acernese et al., 2015). The space-based Laser Interferometer Space Antenna (LISA) (Amaro-Seoane et al., 2017) is anticipated to detect gravitational waves on the 10^{-5} Hz level.

In this study, we use the rapid binary population synthesis code Compact Object Mergers: Population Astrophysics and Statistics (COMPAS) (Stevenson et al., 2017; Vigna-Gómez et al., 2018; Broekgaarden et al., 2019; Neijssel et al., 2019; Riley et al., 2022) to look at neutron star - white dwarf (NSWD) systems. COMPAS implements single stellar evolution (SSE) (Hurley et al., 2000) and binary stellar evolution (BSE) (Hurley et al., 2002). COMPAS takes initial conditions that are set by the user and evolves binary systems to the end of their lifetimes as two compact remnants. COMPAS has been used in similar studies to predict merger rates and other properties (chirp mass, spin, remnant) for DNS and for NSBH systems (Chattopadhyay et al., 2020; Chattopadhyay et al., 2021).

In Section 2, we briefly discuss the pulsar evolution model used in COMPAS. In Section 3, we describe our model results, specifically discussing comparing our model to observation, identified formation channels, comparing radio lifetimes, and analyzing the mass transfer. Finally, in Section 4 we summarize our results.

2 Methods - COMPAS Model

In isolated binary evolution, the pulsar can be assumed to be spinning down due only to its own magnetic dipole, where the rate of change of angular frequency can be described with

$$\dot{\Omega} = -\frac{8\pi B^2 R^6 sin^2\alpha\Omega^3}{3\mu_0 c^3 I} \tag{1}$$

where Ω is the angular frequency, $\dot{\Omega}$ is the first derivative of Ω, B is the surface magnetic field, R is the radius, α is the angle between the axes of rotation and magnetism, c is the speed of light, μ_0 is the permeability of free space, and the I is the moment of inertia. From this we can calculate the values for spin period P and spin-down rate $\dot{P}$, given by

$$P = \frac{2\pi}{\Omega} \tag{2}$$

and

$$\dot{P} = -\frac{\dot{\Omega}P}{\Omega}. \tag{3}$$

At the end of their radio lifetime, pulsars that are powered by their rotation cross a "death line" within the $P\dot{P}$ diagram once the spin of the pulsar has eventually slowed down enough and the pulsar stops emitting in radio. In Figs. 1, 2, and 3, we use the death lines as described in Rudak and Ritter (1994), given by

$$log_{10}\dot{P} = 3.29 \times log_{10}P - 16.55 \tag{4}$$

and

$$log_{10}\dot{P} = 0.92 \times log_{10}P - 18.65 \tag{5}$$

where the second of the death lines is an additional constraint to account for potentially important effects of curvature cooling on electron energy for short-period pulsars ($P < 0.1s$).

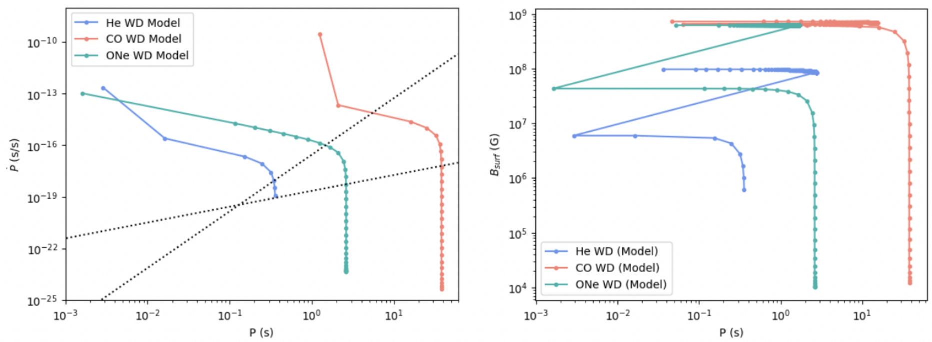

Figure 1: The left panel shows the spin-down rate versus spin period diagram for NSWD systems with three different types of WD companions. This $P\dot{P}$ diagram shows the spin evolution of the neutron stars in these systems. The right panel shows the surface magnetic field versus the spin period (PB), also with the three different types of WD companions. The discontinuous jump from a lower spin period and spin-down rate to a point of higher spin period and spin-down rate shows the phase of mass transfer onto the neutron star from the companion.

In addition to using archival COMPAS data, we also run the updated COMPAS code. In this run, we model 10^5 binary systems with uniform pulsar birth magnetic field and spin period distributions, and with initial masses ranging from 1 M_{sol} to 50 M_{sol}. We use the eccentricity distribution from Sana et al. (2012) and the common envelope mass accretion prescription from MacLeod and Ramirez-Ruiz (2015). However, the results presented in this work are from the archival COMPAS data as the new COMPAS run showed some discrepancies that are still under investigation.

3 COMPAS Model Results

The evolution of a pulsar can be tracked by looking at how the spin period (P) and spin-down rate ($\dot{P}$) evolve together over time, as well as how the spin period and surface magnetic fields (B) evolve together over time. This is visualized in the plots in Fig. 1.

The following sections describe the analysis performed on the resulting model.

3.1 Comparing Model to Observation

To better constrain our models and test for accuracy, we compare the modelled pulsar parameters to observations from the Australia Telescope National Facility pulsar catalogue (ATNF).

In order to compare the COMPAS model to ATNF data of radio pulsars, we must account for radio selection effects in the observations. We use the code PSREvolve (Osłowski et al., 2011) in COMPAS to model the dependence on sky location and the dependence of frequency of scattering/smearing/broadening of the radio beam.

Only after modelling these selection effects can the model be accurately compared to observation. The $P\dot{P}$ diagram of the pulsars in our COMPAS model before and after radio selection effects are accounted for is shown in Fig. 2. A $P\dot{P}$ diagram of the observed pulsars displayed with the COMPAS-modelled population can be seen in Fig. 3.

To compare the observed and modelled distributions, we use the one-dimensional Kolmogorov-Smirnov test to compare individual parameters. We utilize the lower cut-off for the p-value used in Chattopadhyay et al. (2020) (5×10^{-3}) for determining if our distributions can be regarded as strongly dissim-

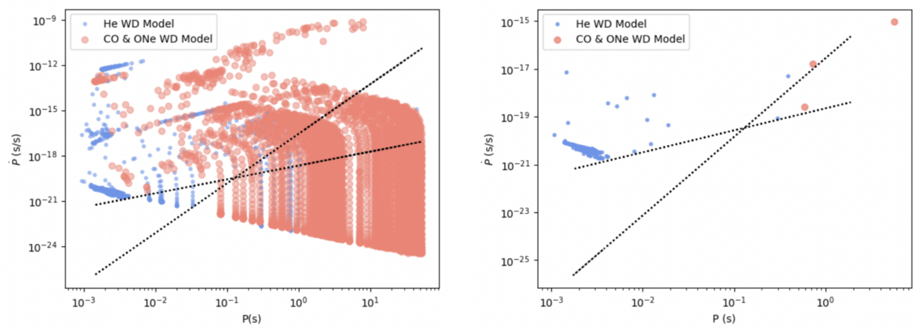

Figure 2: $P\dot{P}$ diagram of NSWD systems with separated WD companion types, from COMPAS model. The left panel shows the model before accounting for radio selection effects, and the right panel shows the model after.

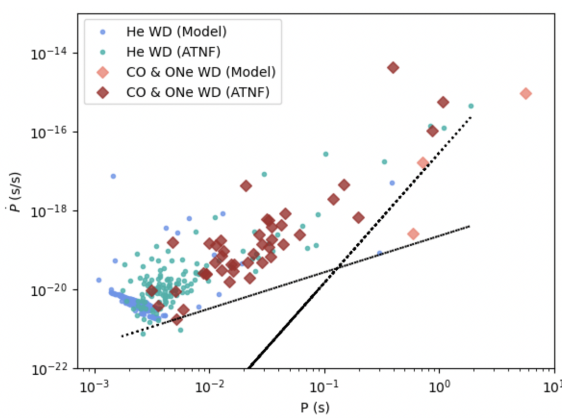

Figure 3: $P\dot{P}$ diagram of the Observational Data from the Australia Telescope National Facility and the COMPAS model of NSWD systems, split into separate WD companion types.

ilar. We find that all of our p-values, for P, $\dot{P}$, B, P_{orb}, and e, are below this limit, for all modelled distributions (Radio alive, SKA observable, Parkes observable) when the populations are split into systems with He and CO(+ONe) WD companion types (we group the modelled CO WDs with the ONe WDs because the ATNF catalogue groups these populations). This suggests that the distributions are entirely dissimilar, and that the specific model used is not in agreement with observation and should be adjusted.

3.2 Formation Channels

From the COMPAS data, the formation channels of the NSWD binary systems can be investigated and visualized with van den Heuvel evolution diagrams. From identifying common patterns, the evolution could be put into one of four different categories of formation depending on the type(s) of mass transfer that occur(s):

(a) **No Mass Transfer (MT)** - Where there is no mass transfer logged in the output files.
(b) **No CE** - Where there is no common envelope phase logged in the output files, but only a Roche lobe overflow phase.
(c) **CE then RLOF** - Where there is a common envelope phase later followed by a Roche lobe overflow phase.
(d) **CE and RLOF** - Where the common envelope and Roche lobe overflow phases are documented to occur almost simultaneously (within 0.001 Myr of each other).

The formation of one binary system for each identified channel is shown in Fig. 4 as separate van den Heuvel diagrams. Fig. 4 shows not only different channels but also different resulting binary systems, three of which show the formation of NSWD systems that contain a CO WD companion, and one of which shows that of NSWD systems that contain a He WD companion. It is noted that these formation channels are not necessarily exclusive to these types of WD companions, but are simply examples of each of these types of channels.

Over all of the NSWD systems modelled, the relative contributions into these four identified channels are shown in Fig. 5. From this we can see that most of the modelled NSWD systems follow the formation channel that involves a RLOF phase but not a CE phase, and out of these systems there is an almost equal split between those with a He WD companion and those with a CO WD companion. This suggests interesting implications on the mass transfer of the binary systems, with the RLOF phase tending to be stable enough to not lead to a CE phase. However, we also notice a significant portion of the systems follow the track where RLOF occurs after CE, suggesting that the CE may not be strongly dependent on a preceding RLOF phase.

3.3 Radio Lifetimes

Post-processing the COMPAS data can distinguish between systems where the NS forms first and where the WD forms first (in this context, denoted NSWD and WDNS, respectively). The differences between the evolution of such systems may be significant, and in particular the differences in the radio lifetimes of the modelled systems can tell us about the formation of millisecond pulsars. With the systems where the neutron star is formed first, the companion star is still evolving and thus more readily transfers its mass unto the neutron star. This mass transfer effectively spins-up the neutron star, as previously described in our Introduction, to the point of radio emission and the creation of a "recycled" pulsar. This spinning-up may continue until the spin period of the pulsar reaches the order of milliseconds, creating what are known as millisecond pulsars. Because of the high spin frequency, these recycled pulsars take longer to slow their spin and thus have a longer radio lifetime. However, in the systems where the white dwarf forms first, less of its mass is available to be transferred to its companion that will evolve to become a neutron star. The neutron star is less spun-up by this mass transfer and does not reach as high of a spin frequency, and the resulting pulsar takes less time to spin-down and thus has a shorter radio lifetime. Fig. 6 shows the birth times of the modelled populations of NSWD and WDNS systems. From this figure, the radio lifetimes of the NSWD systems are significantly longer than those of the WDNS system, as seen by the width of the peak in the radio alive distribution.

3.4 Mass Transfer

Understanding the quantitative amount and the specific type of mass transfer (RLOF, CE, wind accretion, etc.) is critical to understanding the overall formation of NSWD systems, as shown in the different formation channels described in Section 3.2.

The amount of mass transfer can be correlated with the specific type of mass transfer through a mass transfer 'tracker'. One way to investigate this is to look at systems (all binary systems) where the neutron star is formed first, and to see the amount of mass transferred for each process. Fig. 7 shows this data, where one can see that the majority of the systems transfer mass via stable Roche-lobe overflow, and the amount of mass transferred is significant, reaching up to above 1 M_{sol}. This result may indicate that COMPAS is modelling too much of this mode, which may be impacting other results, especially when in comparison to observational data.

4 Conclusions

In this paper, we investigate the formation and evolution of neutron star + white dwarf systems by looking at $P\dot{P}$ diagrams of these systems, with separating the different types of WD companion. We identify and describe several formation channels of these systems, called channels of "No MT", "No CE", "CE then RLOF", and "CE and RLOF". We also find that the archival data shows that the pulsars of the systems where the neutron star forms first have a longer radio lifetime than those in systems where the white dwarf forms first. We lastly find that most of the

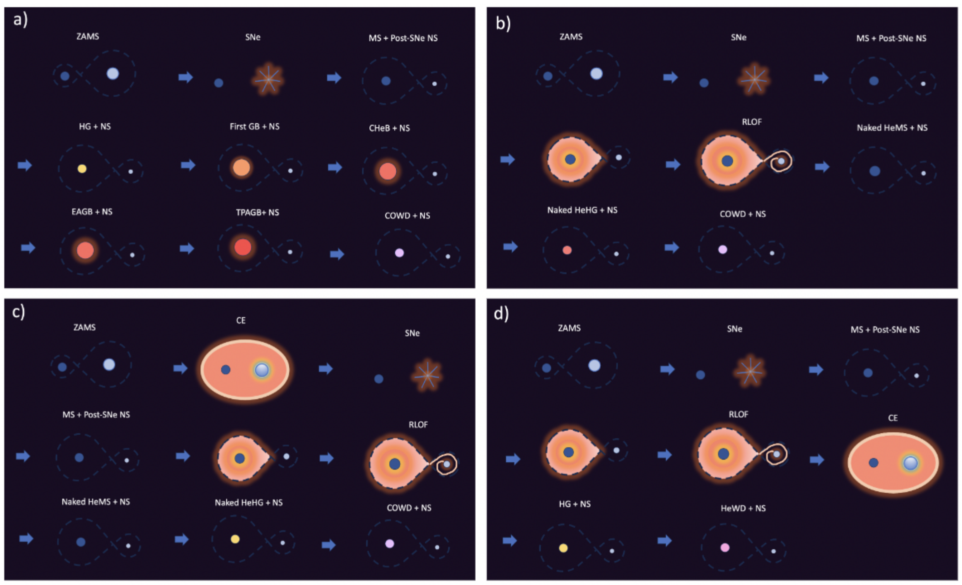

Figure 4: Illustration of the four identified evolutionary channels for the formation of a NSWD system. In panel (a), the NS + COWD system is formed without any logged mass transfer (”No MT” channel). In panel (b), the NS + COWD system is formed through a channel that includes Roche lobe overflow but the system does not experience a common envelope phase (”No CE” channel). Panel (c) shows the evolution of another NS + COWD system, but this includes a common envelope phase which is later followed by a Roche lobe overflow event (”CE then RLOF” channel). Finally, panel (d) shows the evolution of a NS + HeWD through a channel that includes Roche lobe overflow that is logged to occur almost simultaneously as the common envelope phase, which we interpret as the common envelope occurring due to unstable Roche lobe overflow. (”CE and RLOF”) channel

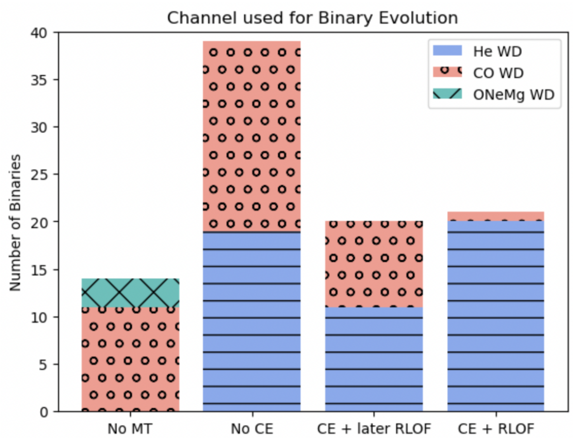

Figure 5: Number of NSWD systems from COMPAS model that follow each identified formation channel, separated into populations with different WD companion types.

mass transfer in the model is from the stable Roche lobe overflow process, and possibly overestimates the amount of mass transfer through this mode. This work may be continued by trying out different COMPAS models to find the best fit in comparison with observational data. From this model, predictions of merger rates may also be used to provide predictions for electromagnetic counterparts of these mergers for future gravitational waves observatories (ex, LISA).

5 Acknowledgments

I would like to thank the National Science Foundation for funding the University of Florida International Research Experiences for Undergraduates program (Grant No. #2348913). I also want to express my gratitude for those at the University of Florida and at Maastricht University for their organizing. I would also like to express my appreciation for Debatri Chattopadhyay and Fabio Antonini for their guidance and mentorship throughout this project. Lastly, thank you to the Gravity Exploration Institute at Cardiff University and the entire IREU cohort for being so welcoming.

6 Data Availability Statement

All of the presented figures in this work were produced by code that can be made readily available upon request.

References

J. Aasi et al. Advanced LIGO. *Classical and Quantum Gravity*, 32(7):074001, Apr. 2015. doi: 10.1088/0264-9381/32/7/074001.

F. Acernese et al. Advanced Virgo: a second-generation interferometric gravitational wave detector. *Classical and Quantum Gravity*, 32 (2):024001, Jan. 2015. doi: 10.1088/0264-9381/32/2/024001.

M. A. Alpar, A. F. Cheng, M. A. Ruderman, and J. Shaham. A new class of radio pulsars. , 300 (5894):728–730, Dec. 1982. doi: 10.1038/300728a0.

P. Amaro-Seoane et al. Laser Interferometer Space Antenna. *arXiv e-prints*, art. arXiv:1702.00786, Feb. 2017. doi: 10.48550/arXiv.1702.00786.

Z. Arzoumanian et al. The NANOGrav 11-year Data Set: High-precision Timing of 45 Millisecond Pulsars. , 235(2):37, Apr. 2018. doi: 10.3847/1538-4365/aab5b0.

D. Bhattacharya and E. P. J. van den Heuvel. Formation and evolution of binary and millisecond radio pulsars. , 203(1-2):1–124, Jan. 1991. doi: 10.1016/0370-1573(91)90064-S.

F. S. Broekgaarden et al. STROOPWAFEL: simulating rare outcomes from astrophysical populations, with application to gravitational-wave sources. , 490(4):5228–5248, Dec. 2019. doi: 10.1093/mnras/stz2558.

D. Chattopadhyay, S. Stevenson, J. R. Hurley, M. Bailes, and F. Broekgaarden. Modelling neutron star-black hole binaries: future pulsar surveys and gravitational wave detectors. , 504(3):3682–3710, July 2021. doi: 10.1093/mnras/stab973.

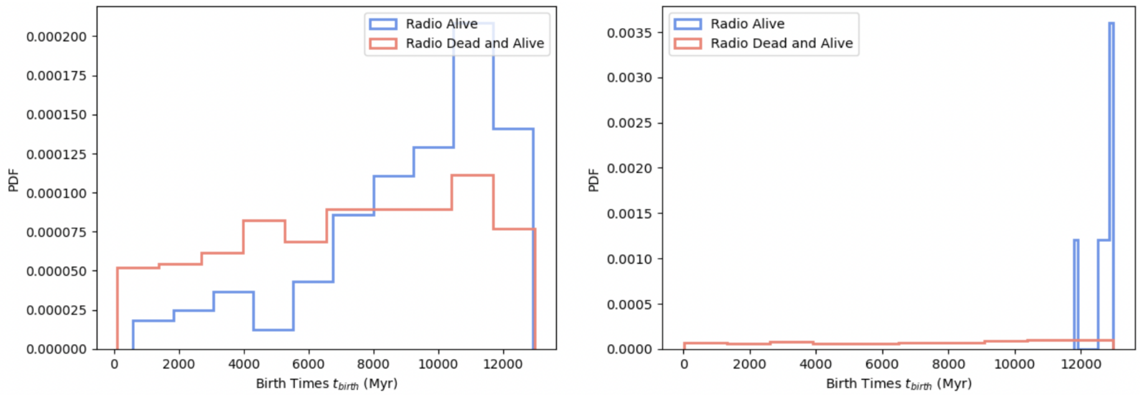

Figure 6: Histogram of the birth times of systems where the NS forms first (left-hand panel) and where the WD forms first (right-hand panel), for populations where the NS is emitting in radio (Radio Alive) and for all NSWD systems (Radio Dead and Alive).

D. Chattopadhyay et al. Modelling double neutron stars: radio and gravitational waves. , 494(2):1587–1610, May 2020. doi: 10.1093/mnras/staa756.

G. Desvignes et al. High-precision timing of 42 millisecond pulsars with the European Pulsar Timing Array. , 458(3):3341–3380, May 2016. doi: 10.1093/mnras/stw483.

A. Hewish, S. J. Bell, J. D. H. Pilkington, P. F. Scott, and R. A. Collins. Observation of a Rapidly Pulsating Radio Source. , 217(5130):709–713, Feb. 1968. doi: 10.1038/217709a0.

G. Hobbs. The parkes pulsar timing array. *Classical and Quantum Gravity*, 30(22):224007, nov 2013. doi: 10.1088/0264-9381/30/22/224007.

G. Hobbs et al. Development of a pulsar-based time-scale. , 427(4):2780–2787, Dec. 2012. doi: 10.1111/j.1365-2966.2012.21946.x.

G. Hobbs et al. A pulsar-based time-scale from the International Pulsar Timing Array. , 491(4):5951–5965, Feb. 2020. doi: 10.1093/mnras/stz3071.

J. R. Hurley, O. R. Pols, and C. A. Tout. Comprehensive analytic formulae for stellar evolution as a function of mass and metallicity. , 315(3):543–569, July 2000. doi: 10.1046/j.1365-8711.2000.03426.x.

J. R. Hurley, C. A. Tout, and O. R. Pols. Evolution of binary stars and the effect of tides on binary populations. , 329(4):897–928, Feb. 2002. doi: 10.1046/j.1365-8711.2002.05038.x.

M. MacLeod and E. Ramirez-Ruiz. Asymmetric Accretion Flows within a Common Envelope. , 803(1):41, Apr. 2015. doi: 10.1088/0004-637X/803/1/41.

C. J. Neijssel et al. The effect of the metallicity-specific star formation history on double compact object mergers. , 490(3):3740–3759, Dec. 2019. doi: 10.1093/mnras/stz2840.

S. Osłowski et al. Population synthesis of double neutron stars. , 413(1):461–479, May 2011. doi: 10.1111/j.1365-2966.2010.18147.x.

V. Radhakrishnan and G. Srinivasan. On the origin of the recently discovered ultra-rapid pulsar. *Current Science*, 51:1096–1099, Dec. 1982.

J. Riley et al. Rapid Stellar and Binary Population Synthesis with COMPAS. , 258(2):34, Feb. 2022. doi: 10.3847/1538-4365/ac416c.

B. Rudak and H. Ritter. The Line of Death - the Line of Birth. , 267:513, Apr. 1994. doi: 10.1093/mnras/267.3.513.

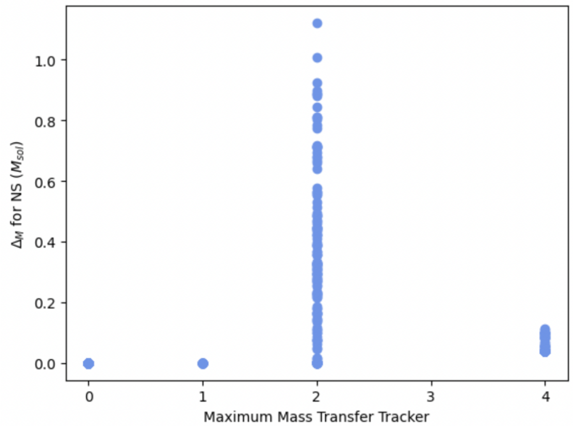

Figure 7: The amount of mass transferred for the different modes of mass transfer. The mass transfer tracker is a variable that keeps track of the mode of mass transfer, where 0 corresponds to no mass transfer, 1 corresponds to common envelope, 2 corresponds to stable Roche lobe overflow, and 4 corresponds to wind accretion.

H. Sana et al. Binary Interaction Dominates the Evolution of Massive Stars. *Science*, 337(6093):444, July 2012. doi: 10.1126/science.1223344.

S. Stevenson et al. Formation of the first three gravitational-wave observations through isolated binary evolution. *Nature Communications*, 8: 14906, Apr. 2017. doi: 10.1038/ncomms14906.

T. M. Tauris, N. Langer, and M. Kramer. Formation of millisecond pulsars with CO white dwarf companions - I. PSR J1614-2230: evidence for a neutron star born massive. , 416(3):2130–2142, Sept. 2011. doi: 10.1111/j.1365-2966.2011.19189.x.

T. M. Tauris, N. Langer, and M. Kramer. Formation of millisecond pulsars with CO white dwarf companions - II. Accretion, spin-up, true ages and comparison to MSPs with He white dwarf companions. , 425(3):1601–1627, Sept. 2012. doi: 10.1111/j.1365-2966.2012.21446.x.

A. Vigna-Gómez et al. On the formation history of Galactic double neutron stars. , 481(3):4009–4029, Dec. 2018. doi: 10.1093/mnras/sty2463.

C. M. Zhang and Y. Kojima. The bottom magnetic field and magnetosphere evolution of neutron star in low-mass X-ray binary. , 366(1):137–143, Feb. 2006. doi: 10.1111/j.1365-2966.2005.09802.x.